Progress In Electromagnetics Research, PIER 80, 179–196, 2008

ENHANCEMENT OF DIRECTIVITY USING 2D-ELECTROMAGNETIC CRYSTALS NEAR THE BAND-GAP EDGE: A FULL-WAVE APPROACH

L. Pajewski, L. Rinaldi, and G. Schettini

Department of Applied Electronics
"Roma Tre" University
Via della Vasca Navale 84, 00146 Roma, Italy

Abstract—A deep analysis of the directivity enhancement, due to the insertion of a simple linear antenna into a dielectric EBG, is presented. The operative frequency is chosen near a band-gap edge. The plane-wave expansion method is used in order to obtain the Bloch dispersion diagrams of infinite two-dimensional EBGs. A rigorous cylindrical-wave approach is used to analyze two-dimensional EBGs with finite size, excited by a line source. We apply these tools to the analysis of different emitting devices, and propose solutions to improve their performances.

1. INTRODUCTION

Electromagnetic crystals [1], also called Electromagnetic Band-Gap (EBG) materials, show an enormous potential in manipulating the propagation of electromagnetic waves. Their technology is advancing rapidly and they are used in a lot of applications, such as waveguides, filters, antennas, high- and low-Q resonators, reflectors, integrated circuits, microstrip structures, lens couplers [2–9].

EBGs are often employed to improve the performances of antennas in the microwave range of frequencies: monopole [10], dipole [11], [12] and wire antennas [13]; slot [14, 15] and patch antennas [15–18]; bow-tie [19], spiral and curl antennas [20]; parabolic reflectors [21]; arrays [22]. In [23], EBG surfaces for effective polarization diversity of wireless communications antenna systems had been optimized using a neural network. In [24], an EBG non-uniform high-impedance surface, imitating the behavior of a perfect magnetic conductor, had been designed for a low-profile antenna. Electromagnetic crystals can be

also employed to reduce mutual coupling between large antenna arrays [25].

In many cases, EBGs are used as planar reflectors, as substrates, or as high impedance ground planes: they are able to eliminate the drawbacks of conducting ground planes, to prevent the propagation of surface waves, to lower the device profiles, and to increase radiation efficiency [11, 26, 27]. Otherwise, EBGs can be employed as superstrates, and their effect is a considerable reduction of the angular range of the field emitted by the antenna [28–30]. Both an electromagnetic-crystal substrate and a cover had been simultaneously used in [31]. Moreover, it had been demonstrated that embedding sources in EBGs working near their band-gap edges it is possible to obtain highly directive antennas [32, 33], thanks to the limited angular propagation allowed within the crystal.

In this work, attention is paid to a class of radiating devices employing EBGs in accordance to the last abovementioned operating mechanism, i.e., on linear antennas whose directivity is controlled and enhanced through the insertion in a dielectric EBG working near a band-gap edge.

The most commonly used techniques for the analysis and design of EBGs are the plane-wave expansion method [1], the finite difference method [34], the finite element method [35], the transfer matrix method [36], and the Fourier modal method [37]. In this paper, the plane-wave expansion method is used to obtain the Bloch dispersion diagrams of infinite two-dimensional EBGs, that are useful to predict the qualitative behavior of an electromagnetic wave propagating in the crystal. In practical applications, the EBG containing the embedded antenna has a finite size and it is excited by an incident field: we model the whole emitting device by means of a rigorous method, representing the field scattered by a finite and periodic set of cylinders in terms of superpositions of cylindrical waves.

The theoretical tools are presented in Section 2. In Section 3 design concepts of highly directive antennas are resumed, numerical examples are given, and solutions are proposed to improve the performances of the emitting devices. In Section 4 some conclusions are drawn.

2. THEORETICAL BACKGROUND

2.1. Electromagnetic Scattering from a 2D-EBG Material Excited by an Electric Line Source

The geometry of our scattering problem is shown in Fig. 1. A finite set of N dielectric circular cylinders, with possibly different radii and

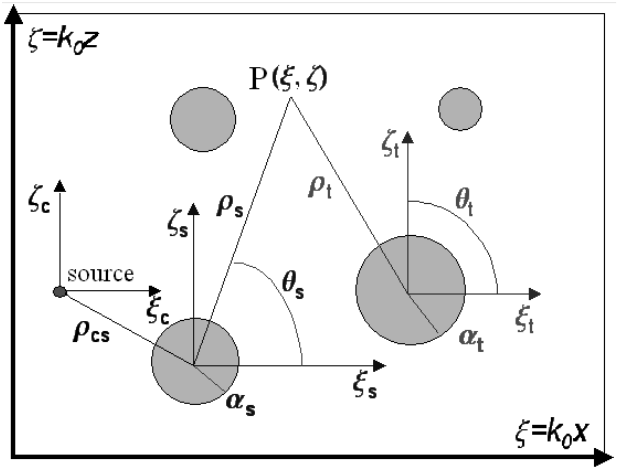

Figure 1. Geometry of the scattering problem.

permittivities, is immersed in a dielectric medium (for the sake of simplicity, we suppose it to be a vacuum). The involved dielectric materials are considered to be linear, isotropic, homogeneous, and lossless. Each cylinder is parallel to the y axis: the structure is assumed to be infinite along the y direction, therefore the problem is reduced to a two-dimensional form. We introduce a main reference frame MRF (O, ξ, ζ), with normalized coordinates $\xi = k_0 x$ and $\zeta = k_0 z$, $k_0 = 2\pi\lambda_0$ being the vacuum wave-number. The electromagnetic excitation is an electric line source, located in (χ_c, η_c) in MRF, and parallel to the axes of the dielectric cylinders. The q-th scatterer has dimensionless radius $\alpha_q = k_0 a_q$, permittivity $\varepsilon_{cq} = \varepsilon_0 n_{cq}^2$, being n_{cq} the refractive index, and axis coordinates (χ_q, η_q) in MRF. Moreover, we introduce N local reference frames RF_q $(q = 1, \ldots, N)$ centered on the cylinder axes: both rectangular (ξ_q, ζ_q) and polar (ρ_q, θ_q) local coordinates are considered, with $\xi_q = k_0 x_q = \xi - \chi_q$, $\zeta_q = k_0 z_q = \zeta - \eta_q$, $\rho_q = k_0 r_q$. The time dependence of the field is assumed to be $e^{-i\omega t}$, where ω is the angular frequency, and is omitted throughout the paper.

The solution to the scattering problem is carried out in terms of $V(\xi, \zeta)$, which represents the y-component of the electric field: $V = E_y(\xi, \zeta)$ for the present $\mathrm{TM}^{(y)}$ case. Once $V(\xi, \zeta)$ is known, it is possible to derive all the other components of the electromagnetic field by using Maxwell's equations.

In order to obtain a rigorous solution for $V(\xi, \zeta)$, the total field is expressed as the superposition of the following three terms, produced by the interaction between incident field and cylinders:

- $V_i(\xi,\zeta)$: incident field;
- $V_s(\xi,\zeta)$: field scattered by the cylinders;
- $V_{cq}(\xi,\zeta)$: field inside the q-th dielectric cylinder.

The incident field V_i can be written as:

$$V_i\left(\xi,\zeta\right) = -V_0 H_0^{(1)}\left(\sqrt{\left(\xi-\chi_c\right)^2+\left(\zeta-\eta_c\right)^2}\right) \tag{1}$$

where V_0 is the incident field amplitude and $H_0^{(1)}$ is the first-kind 0-order Hankel function [38]. In order to facilitate the imposition of the boundary conditions, it is useful to express V_i as a function of RF_q coordinates. To this aim, making use of the addition theorem of Hankel functions [39], we find

$$H_0^{(1)}(\rho_c) = \sum_{\ell=-\infty}^{+\infty} (-1)^\ell H_\ell^{(1)}(\rho_{cq}) e^{i\ell\theta_{cq}} J_\ell(\rho_q) e^{-i\ell\theta_q} \tag{2}$$

where $H_\ell^{(1)}$ is the first-kind Hankel function of integer order ℓ. Therefore, being $(-1)^\ell J_\ell(\cdot) = J_{-\ell}(\cdot)$, and exchanging ℓ with $-\ell$, the incident field becomes

$$V_i\left(\xi_q,\zeta_q\right) = -V_0 \sum_{\ell=-\infty}^{+\infty} CW_{-\ell}(\xi_{cq},\zeta_{cq}) J_\ell(\rho_q) e^{i\ell\theta_q} \tag{3}$$

where $CW_\ell(\xi_{cq},\zeta_{cq}) = H_\ell^{(1)}(\rho_{cq}) e^{i\ell\theta_{cq}}$ is the so-called cylindrical function of integer order ℓ.

The scattered field V_s can be written as the sum of the fields scattered by each cylinder, expressed by a superposition of cylindrical functions with unknown coefficients $c_{h\ell}$:

$$V_s(\xi,\zeta) = V_0 \sum_{t=1}^{N} \sum_{\ell=-\infty}^{+\infty} c_{t\ell} CW_\ell(\xi-\chi_t,\zeta-\eta_t) \tag{4}$$

Making use of the addition theorem of Hankel functions, we can express in the reference frame RF_q, centered on the q-th cylinder, a cylindrical wave emitted by the h-th cylinder, as:

$$H_\ell^{(1)}(\rho_h) e^{i\ell\theta_h} = e^{i\ell\theta_{hq}} \sum_{m=-\infty}^{+\infty} (-1)^m H_{\ell+m}^{(1)}(\rho_{hq}) e^{im\theta_{hq}} J_m(\rho_q) e^{-im\theta_q} \tag{5}$$

After some manipulations, we obtain the following expression for the whole scattered field, in RF_q:

$$V_s(\xi_q,\zeta_q) = V_0 \sum_{m=-\infty}^{+\infty} J_m(\rho_q)e^{im\theta_t} \sum_{h=1}^{N} \sum_{\ell=-\infty}^{+\infty} c_{h\ell} \times \left[CW_{\ell-m}(\xi_{hq},\zeta_{hq})(1-\delta_{hq}) + \frac{H_m^{(1)}(\rho_q)}{J_m(\rho_q)}\delta_{hq}\delta_{m\ell} \right] \quad (6)$$

where δ is the Kronecker symbol.

The field V_{cq} inside the q-th dielectric cylinder is given by an expansion in terms of first-kind Bessel functions, with unknown coefficients d_{qm} [40]:

$$V_{cq}(\xi_q,\zeta_q) = V_0 \sum_{m=-\infty}^{+\infty} i^m e^{-im\varphi_t} d_{qm} J_m(n_{cq}\rho_q)e^{im\theta_q} \quad (7)$$

Once the expressions of all the fields have been given, the boundary conditions on the cylinder surfaces have to be imposed:

$$\begin{cases} V_i(\xi_q,\zeta_q) + V_s(\xi_q,\zeta_q)|_{\rho_q=\alpha_q} = V_{cq}(\xi_q,\zeta_q)|_{\rho_q=\alpha_q} \\ \dfrac{\partial}{\partial\rho_q}\left[V_i(\xi_q,\zeta_q) + V_{\,s}(\xi_q,\zeta_q)\right]\Big|_{\rho_q=\alpha_q} = \dfrac{\partial V_{cq}(\xi_q,\zeta_q)}{\partial\rho_q}\Big|_{\rho_q=\alpha_q} \end{cases} \quad (8)$$

where $q = 1,\ldots,N$.

By using the orthogonality property of the exponential functions, after some manipulations, it is possible to obtain a linear system for the unknown coefficients $c_{h\ell}$ and d_{qm}:

$$\begin{cases} \displaystyle\sum_{h=1}^{N}\sum_{\ell=-\infty}^{+\infty} A_{m\ell}^{hq(1)} c_{h\ell} - B_m^{q(1)} = d_{qm} G_m^{q(1)} \\ \displaystyle\sum_{h=1}^{N}\sum_{\ell=-\infty}^{+\infty} A_{m\ell}^{hq(2)} c_{h\ell} - B_m^{q(2)} = d_{qm} G_m^{q(2)} \end{cases} \quad (9)$$

with $m = 0, \pm1, \pm2, \ldots$, $q = 1,\ldots,N$, and

$$A_{m\ell}^{hq} = \left[CW_{\ell-m}(\xi_{ht},\zeta_{ht})(1-\delta_{hq})\right] T_m(\alpha_q) + \delta_{hq}\delta_{\ell m} \quad (10)$$

$$B_m^q = T_m(\alpha_q) CW_{-m}(\xi_{cq},\zeta_{cq}) \quad (11)$$

$$G_m^{q(1)} = J_m(n_{cq}\alpha_q)/H_m^{(1)}(\alpha_q) \quad (12)$$

$$G_m^{q(2)} = n_{cq} J_m{}'(n_{cq}\alpha_q)/H_m^{(1)\prime}(\alpha_q) \quad (13)$$

where $T_m^{(1)}(x) = J_m(x)/H_m^{(1)}(x)$ and $T_m^{(2)}(x) = J_m{}'(x)/H_m^{(1)\prime}(x)$.

A way to solve the system (9) is to eliminate the coefficients d_{qm}, thus obtaining a linear system for the sole $c_{h\ell}$ coefficients. From Eqs. (9) it follows

$$d_{qm} = \frac{\sum_{h=1}^{N}\sum_{\ell=-\infty}^{+\infty} A_{m\ell}^{hq(1)} c_{h\ell} - B_m^{q(1)}}{G_m^{q(1)}} = \frac{\sum_{h=1}^{N}\sum_{\ell=-\infty}^{+\infty} A_{m\ell}^{hq(2)} c_{h\ell} - B_m^{q(2)}}{G_m^{q(2)}} \quad (14)$$

therefore

$$\sum_{h=1}^{N}\sum_{\ell=-\infty}^{+\infty} D_{m\ell}^{hq} c_{h\ell} = M_m^q \quad (15)$$

where $D_{m\ell}^{hq} = G_m^{q(2)} A_{m\ell}^{hs(1)} - G_m^{q(1)} A_{m\ell}^{hq(2)}$, and $M_m^q = B_m^{q(1)} L_m^{q(2)} - B_m^{q(2)} L_m^{q(1)}$.

By knowledge of the $c_{h\ell}$ and d_{qm} coefficients, the total electromagnetic field is completely determined in any point of space.

Although no approximations have been introduced in the theoretical analysis, to obtain numerical results it is necessary to approximate the series in Eqs. (9) with a finite number of terms. The choice of a truncation index $M \cong 3n_1\alpha$, where α is the maximum dimensionless radius α_q ($q = 1, \ldots, N$), usually reveals an efficient criterion, showing a good compromise between accuracy and computational heaviness [41]. However, in all the performed computations we required a convergence on the third significant figure: to this aim, in some cases we used larger values of M.

2.2. Plane-wave Expansion Method and Bloch Dispersion Diagrams

The study of infinite electromagnetic crystals properties is often based on Bloch modes dispersion diagrams, which describe the intrinsic properties of the periodic structures in the absence of any incident field, and give information about the possible energy propagation directions.

We computed the dispersion diagrams by using a plane wave expansion method. In particular, according to the Bloch theorem, we write the electric field $V(x, z)$ as

$$V(x, z) = e^{ik_{0x}x} e^{ik_{0z}z} V_p(x, z) \quad (16)$$

where $k_{0x} = k_0 \cos\theta$, $k_{0z} = k_0 \sin\theta$, θ being the generic propagation angle (see Figure 2(a)), and $V_p(x, z)$ is a periodic function that can be

expanded in a Fourier series, as follows:

$$V_p(x,z) = \sum_{n=-\infty}^{+\infty} \sum_{q=-\infty}^{+\infty} V_{nq} e^{i\frac{2\pi nx}{d_x}} e^{i\frac{2\pi qz}{d_z}} \tag{17}$$

where d_x and d_z are the periods of the electromagnetic crystal along x and z directions, respectively.

Also the inverse of the relative permittivity of the EBG, $\varepsilon_r^{-1}(x,z)$, is a periodic function, and it can be expanded in a Fourier series:

$$\varepsilon_r^{-1}(x,z) = \sum_{m=-\infty}^{+\infty} \sum_{p=-\infty}^{+\infty} \zeta_{mp} e^{i\frac{2\pi mx}{d_x}} e^{i\frac{2\pi pz}{d_z}} \tag{18}$$

From Helmholtz equation $\nabla^2 \mathbf{V} + \varepsilon_r k_0^2 \mathbf{V} = 0$ it follows

$$\frac{1}{\varepsilon_r}\left(\frac{\partial^2 V}{\partial x^2} + \frac{\partial^2 V}{\partial z^2}\right) + k_0^2 V = 0 \tag{19}$$

By substituting Eqs. (16)–(18) in Eq. (19), one obtains:

$$\sum_{n=-\infty}^{+\infty} \sum_{q=-\infty}^{+\infty} \sum_{m=-\infty}^{+\infty} \sum_{p=-\infty}^{+\infty} \left[\left(\frac{2\pi nx}{d_x} + k_{0x}\right)^2 + \left(\frac{2\pi qz}{d_z} + k_{0z}\right)^2\right] \times$$
$$\zeta_{mp} e^{i\frac{2\pi mx}{d_x}} e^{i\frac{2\pi pz}{d_z}} V_{nq} e^{i\frac{2\pi nx}{d_x}} e^{i\frac{2\pi qz}{d_z}} + k_0^2 \sum_{n=-\infty}^{+\infty} \sum_{q=-\infty}^{+\infty} V_{nq} e^{i\frac{2\pi nx}{d_x}} e^{i\frac{2\pi qz}{d_z}} = 0 \tag{20}$$

Multiplying for $e^{-i\frac{2\pi fx}{d_x}} e^{-i\frac{2\pi \ell z}{d_z}}$, and integrating on d_x and d_z, the following eigenvalue equation is found

$$\sum_{n=-\infty}^{+\infty} \sum_{q=-\infty}^{+\infty} V_{nq} \zeta_{f-n,\ell-q} \left[\left(\frac{2\pi nx}{d_x} + k_{0x}\right)^2 + \left(\frac{2\pi qz}{d_z} + k_{0z}\right)^2\right] + k_0^2 V_{f\ell} = 0 \tag{21}$$

In the classical presentation of Bloch diagrams, the solutions for the Bloch wave-vector $\mathbf{k}(\omega)$ are presented on a two-dimensional plot, where the abscissa represents the edge of the first reduced Brillouin zone. We give in Figure 2(b) an example of such diagram in the case of an EBG made of circular-section rods of radius $a = 0.23\,\text{cm}$ and refractive index $n_c = 2.9$, lying in a vacuum, arranged on a triangular lattice with $d_x = d_z = 1.51\,\text{cm}$, sketched in Figure 2(a).

Most of the information about waves propagating in an infinite EBG can be deduced from a two-dimensional dispersion diagram.

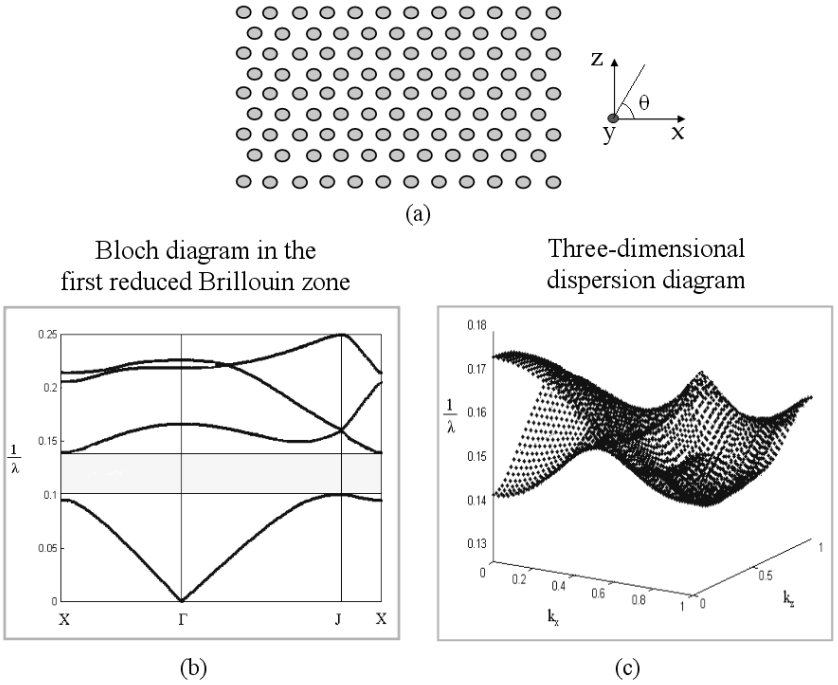

Figure 2. (a) Sketch of an EBG made of dielectric circular-section rods arranged on a triangular lattice. (b) Bloch modes dispersion two-dimensional diagram along the edge of the first reduced Brillouin zone, for the crystal of (a) when the rods have radius $a = 0.23\,\text{cm}$ and refractive index $n_c = 2.9$, the periods of the lattice are $d_x = d_z = 1.51\,\text{cm}$ along x and z. (c) Bloch modes dispersion three-dimensional diagram in the whole Brillouin zone, for the same crystal of (b).

However, a three-dimensional plot in which the Bloch wavevector covers the whole Brillouin zone, instead of the edge of the first reduced one, reveals more completely the EBG dispersion relation properties: an example of such diagram is given in Figure 2(c), for the same structure as in Figure 2(a). Each band is represented by a curved sheet: in order to obtain the customary two-dimensional view, one should intersect the sheets with the vertical walls of a prism whose base is the first Brillouin zone. The intersection of the sheets with a horizontal plane corresponding to the operation wavelength, instead, gives a curve in the (k_x, k_y) plane, that is a constant-frequency dispersion diagram that turns out to be useful in the design of directive antennas.

3. DESIGN OF DIRECTIVE ANTENNAS

A source embedded inside an electromagnetic crystal, working at a frequency corresponding to a band-gap edge, constitutes an antenna radiating energy in a very narrow angular range.

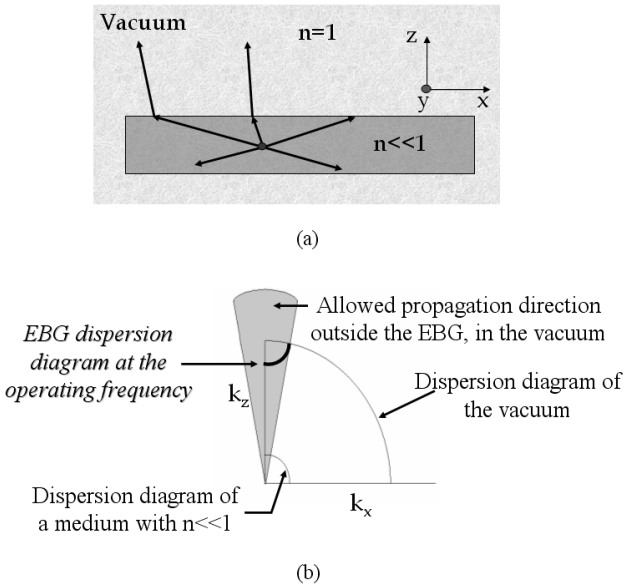

Figure 3. Schematic drawings illustrating concepts of propagation outside an EBG working near a band-gap edge.

An EBG near a band-gap edge may behave like a homogeneous dielectric material with refractive index $n \ll 1$ (see Figure 3(a)) [42]. The constant-frequency dispersion curve of a vacuum is a circle defined by $k_x^2 + k_z^2 = k_0^2$, the corresponding curve of a material with $n \ll 1$ is a circle with a smaller radius (see Figure 3(b)). If we want to enforce the radiated field inside a small angular range centered around the z axis, the constant-frequency dispersion curve of the EBG should entirely lay inside the gray region in Figure 3(b): it corresponds to large k_z values and small k_x values. This can be obtained working at a frequency near a band-gap edge, and appropriately expanding the unit cell of the crystal in the z direction. A detailed explanation can be found in [32].

In Figure 4(b), we report the polar radiated pattern for a finite EBG structure with 92 circular-section rods of radius $a = 0.23$ cm and refractive index $n_c = 2.9$, lying in a vacuum, arranged on a triangular lattice with periods $d_x = 1.51$ cm and $d_z = 1.48$ cm, excited by a wire

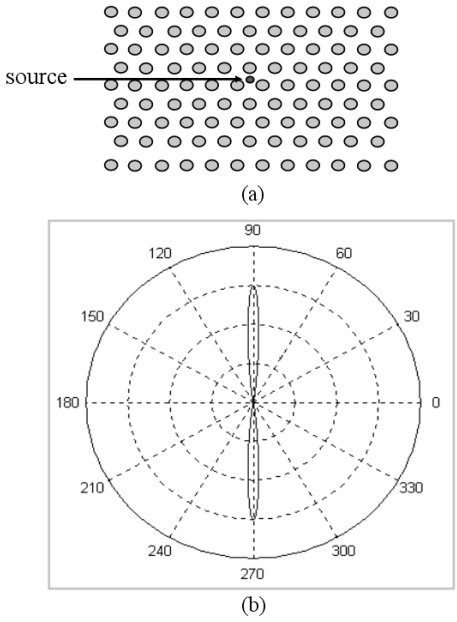

Figure 4. (a) Geometry of a finite EBG with 92 circular-section rods lying in a vacuum, arranged on a triangular lattice and excited by a wire source. (b) Polar radiated pattern for the structure of (a) when $a = 0.23\,\mathrm{cm}$, $n_c = 2.9$, $d_x = 1.51\,\mathrm{cm}$, $d_z = 1.48\,\mathrm{cm}$; the operating frequency is $f = 10\,\mathrm{GHz}$.

source positioned as shown in Figure 4(a). The operating frequency is $f = 10\,\mathrm{GHz}$: it is inside a gap for the infinite crystal of Figure 2, but it is on a gap-edge for the finite and expanded crystal now considered. Because of the symmetry with respect to the x axis, the radiation occurs for both $+z$ and $-z$ directions, in a narrow angular range. If only the $+z$ lobe is considered, as if the $-z$ lobe was not present, the directivity of the device turns out to be $D = 19.7\,\mathrm{dB}$, the side lobe level is $SLL = -17.3\,\mathrm{dB}$, and the half power beam width is $HPBW = 9.5°$.

In order to avoid the radiation along $-z$ direction, a ground plane or a mirror could be used. Another possible solution is using an EBG as a mirror, i.e., placing beside the above described structure a different EBG, showing a stop-band at the operating frequency. In Figure 5(b) we report the polar pattern for the same structure as in Figure 4, placed beside a 57 circular-section rod EBG with $a = 0.23\,\mathrm{cm}$, $n_c = 2.9$, and with periods $d_x = 1.51\,\mathrm{cm}$ and $d_{z1} = 1.31\,\mathrm{cm}$, along x and z, respectively: the whole device is sketched in Figure 5(a). Only the

$+z$ radiation lobe is now present; it is narrower than the two lobes of Figure 4, in fact it is now found that $D = 21.7\,\text{dB}$, $SLL = -17.3\,\text{dB}$, and $HPBW = 8.4°$.

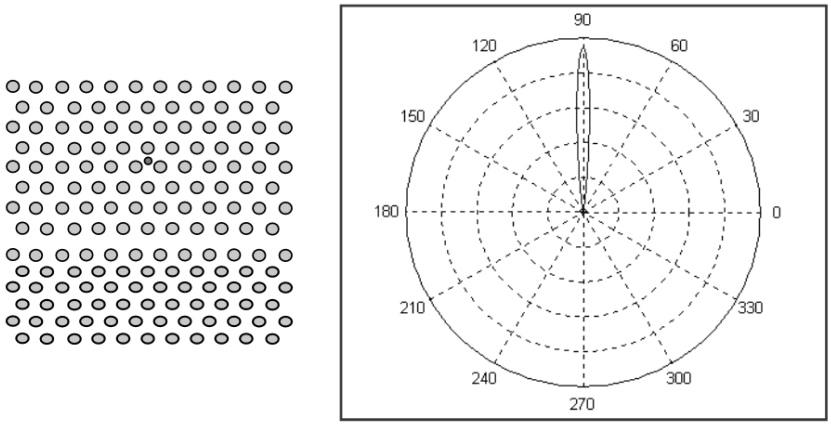

(a) (b)

Figure 5. (a) Geometry of the same EBG as in Figure 4 placed beside a 57 circular-section rods EBG with different z-period d_{z1}. (b) Polar radiated pattern for the structure of (a) when $d_{z1} = 1.31\,\text{cm}$.

In order to improve the antenna performances, it appears that the lateral size of the EBG has to be widened [19]. The structure sketched in Figure 6(a) is similar to the one considered in Figure 5, but now 273 cylinder are present. Being the structure larger along x, the field shows more significant transverse variations inside the EBG, consequently a radiated pattern with higher lateral lobes is obtained. However, if the periods along z are slightly shortened in order to get closer to the band-gap edge (as an alternative, the operating frequency could be slightly reduced), the corresponding constant-frequency dispersion diagram becomes a smaller closed curve and the allowed k_x of the Bloch wave vector become smaller too: therefore, the spatial variations of the field along x become again smooth. The following values for the antenna parameters are found, when $d_z = 1.47$ and $d_{z1} = 1.30$: $D = 22.5\,\text{dB}$, $SLL = -25\,\text{dB}$, and $HPBW = 6.6°$.

In the design of this kind of antennas, the reduction of the device size is an important goal. To this aim, we considered alternative configurations. In the following, we present preliminary results concerning a triangular set of 49 circular-section rods of radius $a = 0.26\,\text{cm}$ and refractive index $n_c = 3$, lying in a vacuum, arranged on

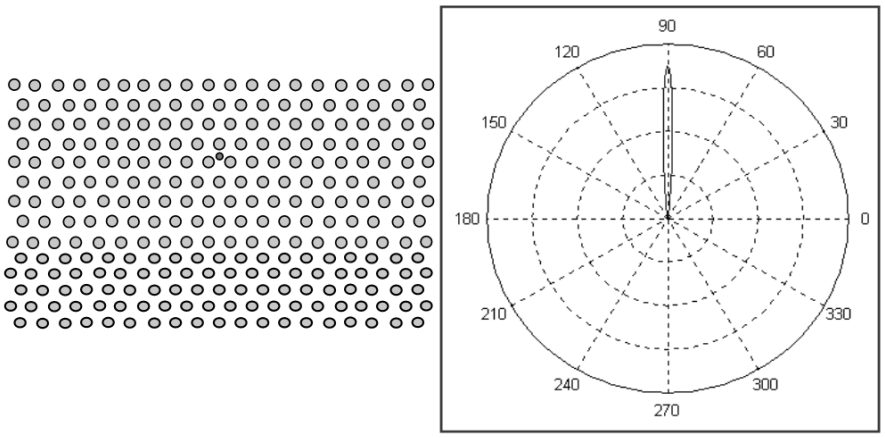

(a) (b)

Figure 6. (a) Geometry of an EBG similar to the one considered in Figure 5 but widened along x direction: 273 cylinder are now present. (b) Polar radiated pattern for the structure of (a) when $d_z = 1.47\,\text{cm}$ and $d_{z1} = 1.30\,\text{cm}$.

a square lattice with $d_x = d_z = 1.48\,\text{cm}$, and excited by a wire source positioned as shown in Figure 7(a). The operating frequency is $f = 10\,\text{GHz}$, and it is on a gap-edge for the square-lattice electromagnetic crystal now considered. The polar radiated pattern is reported in Figure 7(b), it is narrow along $+z$ direction but it is large and indented along $-z$ direction.

Placing next to the structure of Figure 7 a triangular set of 36 circular-section rods of radius $a = 0.26\,\text{cm}$ and refractive index $n_c = 3$, arranged on a rectangular lattice with periods $d_x = 1.48\,\text{cm}$ and $d_{z1} = 1.31\,\text{cm}$, as shown in Figure 8(a), the radiation along $-z$ direction can be avoided. The corresponding polar pattern is reported in Figure 8(b) and the following antenna parameters are calculated: $D = 18\,\text{dB}$, $SLL = -16\,\text{dB}$, and $HPBW = 9.3°$.

In order to improve the antenna performances, the lateral size of the EBG has to be widened and the periods along z slightly shortened, as previously discussed. In Figure 9 the upper triangular EBG in which the source is embedded has $d_x = d_z = 1.45\,\text{cm}$ (in order to maintain the lattice squared, even the period along x has been shortened), the lower EBG has $d_x = 1.45\,\text{cm}$ and $d_{z1} = 1.29\,\text{cm}$. Moreover, for all the cylinders $a = 0.26\,\text{cm}$ and $n_c = 3$. The total number of cylinders is now 157. For this device it is found that $D = 21\,\text{dB}$, $SLL = -18\,\text{dB}$,

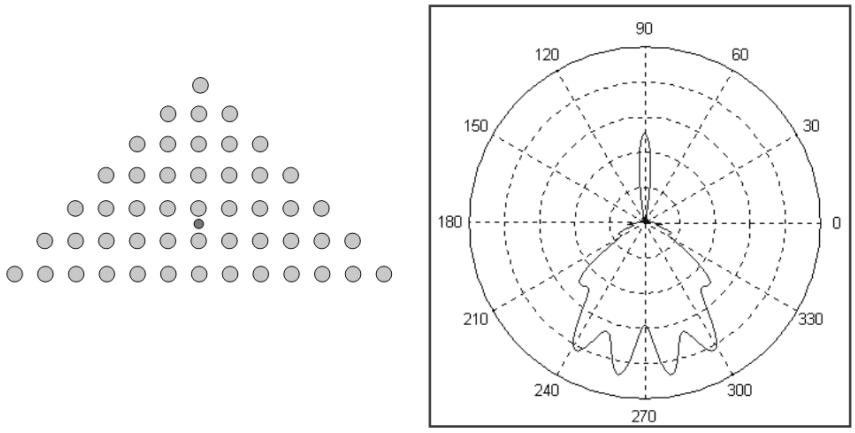

(a) (b)

Figure 7. (a) Geometry of a finite triangular EBG with 49 circular-section rods lying in a vacuum, arranged on a square lattice and excited by a wire source. (b) Polar radiated pattern for the structure of (a) when $a = 0.26\,\text{cm}$, $n_c = 3$, $d_x = d_z = 1.48\,\text{cm}$; the operating frequency is $f = 10\,\text{GHz}$.

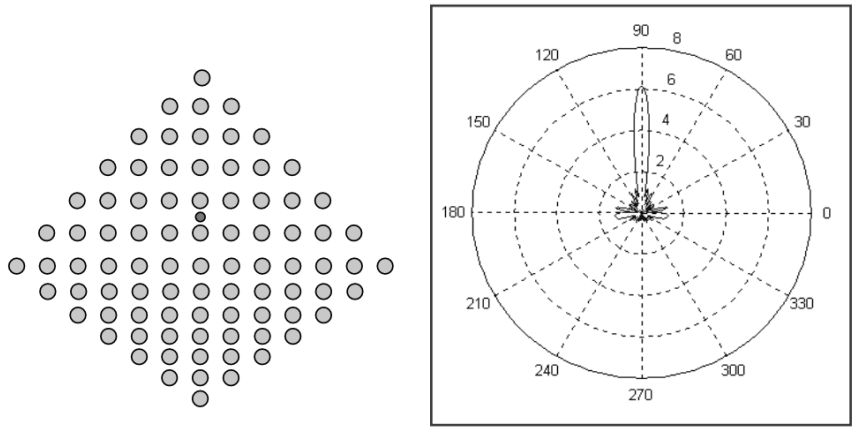

(a) (b)

Figure 8. (a) Geometry of the same EBG as in Figure 7 placed beside a 36 circular-section rods EBG with different period d_{z1}. (b) Polar radiated pattern for the structure of (a) when $d_{z1} = 1.31\,\text{cm}$.

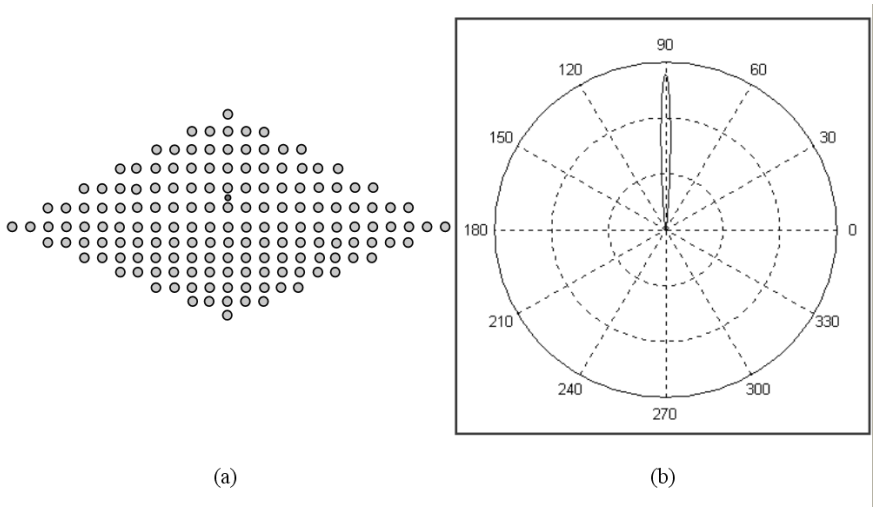

Figure 9. (a) Geometry of an EBG similar to the one considered in Figure 8 but widened along x direction: 157 cylinder are now present. (b) Polar radiated pattern for the structure of (a) when $d_x = d_z = 1.45\,\text{cm}$ and $d_{z1} = 1.29\,\text{cm}$.

and $HPBW = 8.5°$. This results can be compared with those of the antenna of Figure 6: the performances of the triangular antenna are good, and the adoption of a triangular configuration allows to half the number of cylinders.

4. CONCLUSIONS

In this paper, we studied a class of radiating devices with enhanced directivity. The enhancement mechanism is based on the insertion of the source in a dielectric EBG working near a band-gap edge. We implemented the plane-wave expansion method to obtain the Bloch dispersion diagrams of infinite two-dimensional EBGs. We have studied the directive spectral properties of the electromagnetic crystal. A cylindrical-wave approach was developed to analyze two-dimensional EBGs with finite size, excited by a line source.

We presented numerical results, concerning different emitting devices, and proposed solutions to improve their performances. A natural direction for future work seems us to be an accurate optimization of the EBG geometrical parameters and of the source position, in order to improve the performances of the antennas presented in this paper, or to find better geometries.

REFERENCES

1. Joannopoulos, J. D., R. D. Meade, and J. N. Winn, *Photonic Crystals: Molding the Flow of Light*, Princeton University Press, Princeton, NJ, 1995.
2. De Maagt, P., R. Gonzalo, Y. C. Vardaxoglou, and J.-M. Baracco, "Electromagnetic bandgap antennas and components for microwave and (sub)millimeter wave applications," *IEEE Trans. Antennas Propag.*, Vol. 51, No. 10, 2667–2677, Oct. 2003.
3. Fernandes, H. C. C., J. L. G. Medeiros, M. A. Isnaldo, Jr., and D. B. Brito, "Photonic crystal at millimeter waves applications," *PIERS Online*, Vol. 3, 689–694, 2007.
4. Qi, L., Z. Yang, Z. Liang, W. Liu, Y. Liu, and X. Gao, "Design of photonic crystal resonant cavity using overmoded dielectric photonic band gap structures," *PIERS Online*, Vol. 3, 379–381, 2007.
5. Luan, P.-G. and K.-D. Chang, "Photonic-crystal lens coupler using negative refraction," *PIERS Online*, Vol. 3, 91–95, 2007.
6. Fernandes, H. C. C. and G. D. F. Alves, "Multilayer planar resonators with superconductive patch on PBG substrate," *PIERS Online*, Vol. 3, 560–563, 2007.
7. Hwang, C. G. and N. H. Myung, "Novel phase noise reduction and harmonic improvement methods of an oscillator utilizing a CCPW EBG structure," *PIERS Proceedings*, 16–20 (Session 1A4), Tokyo, Japan, August 2–5, 2006.
8. Fernandes, H. C. C., D. B. Brito, and J. L. G. Medeiros, "EBG substrate in unilateral fin line resonator," *PIERS Proceedings*, 530–534, Prague, Czech Republic, August 27–30, 2007.
9. Tomljenovic-Hanic, S., C. M. de Sterke, M. J. Steel, and D. J. Moss, "Design of high-Q cavities in photosensitive material-based photonic crystal slab heterostructures," *PIERS Online*, Vol. 3, 233–235, 2007.
10. Boutayeb, H. and T. A. Denidni, "Analysis and design of a high-gain antenna based on metallic crystals," *Journal of Electromagnetic Waves and Applications*, Vol. 20, 599–614, 2006.
11. Sigalas, M. M., R. Biswas, Q. Li, D. Crouch, W. Leung, R. Jacobs-Woodbury, B. Lough, S. Nielsen, S. McCalmont, G. Tuttle, and K. M. Ho, "Dipole antennas on photonic band-gap crystals — Experiment and simulation," *Microwave and Opt. Technol. Lett.*, Vol. 15, 153–158, 1997.
12. Yang, F., V. Demir, D. A. Elsherbeni, A. Z. Elsherbeni, A. A. Eldek, "Enhancement of printed dipole antennas characteristics us-

ing semi-EBG ground plane," *Journal of Electromagnetic Waves and Applications*, Vol. 20, No. 8, 993–1006, 2006.

13. Yang, F. and Y. Rahmat-Samii, "Reflection phase characterizations of the EBG ground plane for low profile wire antenna applications," *IEEE Trans. Antennas Propag.*, Vol. 51, No. 10, 2691–2703, Oct. 2003.
14. Leung, W. Y., R. Biswas, S. D. Cheng, M. M. Sigalas, J. S. McCalmont, G. Tuttle, and K. M. Ho, "Slot antennas on photonic band gap crystals," *IEEE Trans. Antennas Propag.*, Vol. 45, No. 8, 1569–1570, Aug. 1997.
15. Weily, A. R., L. Horvath, K. P. Esselle, B. C. Sanders, and T. S. Bird, "A planar resonator antenna based on a woodpile EBG material," *IEEE Trans. Antennas and Propagat.*, Vol. 53, No. 1, 216–223, Jan. 2005.
16. Gonzalo, R., P. de Maagt, and M. Sorolla, "Enhanced patch-antenna performance by suppressing surface waves using photonic-bandgap substrates," *IEEE Trans. on Microwave Theory Tech.*, Vol. 47, No. 11, 2131–2138, Nov. 1999.
17. Coccioli, R., F. Yang, K. Ma, and T. Itoh, "Aperture-coupled patch antenna on UC-PBG substrate," *IEEE Trans. on Microwave Theory Tech.*, Vol. 47, No. 11, 2123–2130, Nov. 1999.
18. Colburn, J. S. and Y. Rahmat-Samii, "Patch antennas on externally perforated high dielectric constant substrates," *IEEE Trans. Antennas Propagat.*, Vol. 47, No. 12, 1785–1794, Dec. 1999.
19. Brown, E. R., C. D. Parker, and E. Yablonovith, "Radiation properties of a planar antenna on a photonic-crystal substrate," *J. Opt. Soc. Am. B*, Vol. 10, No. 2, 404–407, Feb. 1993.
20. Yang, F. and Y. Rahmat-Samii, "A low profile circularly polarized curl antenna over an electromagnetic bandgap (EBG) surface," *Microw. Opt. Tech. Lett.*, Vol. 31, No. 4, 264–267, Nov. 2001.
21. Thevenot, M., A. Reineix, and B. Jecko, "A dielectric photonic parabolic reflector," *Microw. Opt. Tech. Lett.*, Vol. 21, No. 6, 411–414, June 1999.
22. Li, L., C. H. Liang, and C. H. Chan, "Waveguide end-slot phased array antenna integrated with electromagnetic bandgap structures," *Journal of Electromagnetic Waves and Applications*, Vol. 21, No. 2, 161–174, 2007.
23. Ganatsos, T., K. Siakavara, and J. N. Sahalos, "Neural network-based design of EBG surfaces for effective polarization diversity of wireless communications antenna systems," *PIERS Online*, Vol. 3, No. 8, 1165–1169, 2007.

24. Hosseini, M., A. Pirhadi, and M. Hakkak, "Design of a non-uniform high impedance surface for a low profile antenna," *PIERS Proceedings*, 352–356, Cambridge, USA, March 26–29, 2006.
25. Fu, Y. Q., Q. R. Zheng, Q. Gao, and G. H. Zhang, "Mutual coupling reduction between large antenna arrays using electromagnetic bandgap (EBG) structures," *Journal of Electromagnetic Waves and Applications*, Vol. 20, No. 6, 819–825, 2006.
26. Gonzalo, R., P. de Maagt, and M. Sorolla, "Enhanced patch-antenna performance by suppressing surface waves using photonic-bandgap substrates," *IEEE Trans. on Microwave Theory Tech.*, Vol. 47, No. 11, 2131–2138, Nov. 1999.
27. Yang, H. Y. D., N. G. Alexopoulos, and E. Yablonovitch, "Photonic band-gap materials for high-gain printed circuit antennas," *IEEE Trans. on Antennas and Propagat.*, Vol. 45, No. 1, 185–187, Jan. 1997.
28. Thevenot, M., C. Cheype, A. Reineix, and B. Jecko, "Directive photonic-bandgap antennas," *IEEE Trans. Microwave Theory Tech.*, Vol. 47, No. 11, 2115–2122, Nov. 1999.
29. Cheype, C., C. Serier, M. Thevenot, T. Monediere, A. Reineix, and B. Jecko, "An electromagnetic bandgap resonator antenna," *IEEE Trans. Antennas Propagat.*, Vol. 50, No. 9, 1285–1290, Sept. 2002.
30. Frezza, F., L. Pajewski, P. Nocito, and G. Schettini, "FDTD analysis of EBG superstrates," *2007 IEEE Workshop on Computational Electromagnetics in Time-Domain (CEM-TD)*, 4, Perugia, Oct. 15–17, 2007.
31. Qiu, M. and S. He, "High-directivity patch antenna with both photonic bandgap substrate and photonic cover," *Microw. Opt. Tech. Lett.*, Vol. 30, No. 1, 41–44, July 2001.
32. Enoch, S., G. Tayeb, and D. Maystre, "Dispersion diagrams of Bloch modes applied to the design of directive sources," *Progress In Electromagnetic Research*, PIER 37, 61–81, 2002.
33. Enoch, S., G. Tayeb, P. Sabouroux, N. Guérin, and P. Vincent, "A meta-material for directive emission," *Phys. Rev. Lett.*, Vol. 89, No. 21, 213902, Nov. 2002.
34. Liu, Y., Z. Yang, Z. Liang, and L. Qi, "A memory-efficient strategy for the FDTD implementation applied to the photonic crystals problems," *PIERS Online*, Vol. 3, 374–378, 2007.
35. Lin, M.-C. and R.-F. Jao, "Finite element analysis of photon density of states for two-dimensional photonic crystals with in-

plane light propagation," *PIERS Online*, Vol. 3, 315–319, 2007.

36. Pendry, J. B. and A. MacKinnon, "Calculation of photon dispersion relations," *Phys. Rev. Lett.*, Vol. 69, 2772–2775, 1992.
37. Frezza, F., L. Pajewski, and G. Schettini, "Characterization and design of two-dimensional electromagnetic band-gap structures by use of a full-wave method for diffraction gratings," *IEEE Transactions on Microwave Theory and Techniques*, Vol. 51, No. 3, 941–951, 2003.
38. Abramowitz, M. and I. Stegun, *Handbook of Mathematical Functions*, Dover, New York, 1972.
39. Sneddon, I. N., *Mixed Boundary Value Problems in Potential Theory*, North-Holland, Amsterdam, 1966.
40. Balanis, C. A., *Advanced Engineering Electromagnetics*, John Wiley and Sons, New York, 1989.
41. Di Vico, M., F. Frezza, L. Pajewski, and G. Schettini, "Scattering by a finite set of perfectly conducting cylinders buried in a dielectric half-space: a spectral-domain solution," *IEEE Trans. on Antennas and Propagat.*, Vol. 53, No. 2, 719–727, Feb. 2005.
42. Engheta, N. and R. W. Ziolkowski, *Metamaterials: Physics and Engineering Explorations*, Wiley-IEEE Press, 2006.